Mineralogy and Petrology
https://doi.org/10.1007/s00710-018-0647-y

ORIGINAL PAPER

Murashkoite, FeP, a new terrestrial phosphide from pyrometamorphic rocks of the Hatrurim Formation, South Levant

Sergey N. Britvin[1,2] · Yevgeny Vapnik[3] · Yury S. Polekhovsky[1] · Sergey V. Krivovichev[1,2] · Maria G. Krzhizhanovskaya[1] · Liudmila A. Gorelova[1] · Oleg S. Vereshchagin[1] · Vladimir V. Shilovskikh[4] · Anatoly N. Zaitsev[1]

Received: 20 July 2018 / Accepted: 8 November 2018

Abstract

Murashkoite, FeP, is a new mineral found in pyrometamorphic rocks of the Hatrurim Formation, South Levant. It is a typical accessory phase in the marbles and paralavas in the southern Negev Desert, Israel and on the Transjordan Plateau, Jordan. Murashkoite occurs as grains and aggregates up to 2 mm closely associated with barringerite, $(Fe,Ni)_2P$, and zuktamrurite, FeP_2. The rock-forming minerals include pyroxenes of the diopside-hedenbergite series, anorthite with subordinate gehlenite, tridymite, cristobalite, pyrrhotite, fluorapatite, chromite, magnetite, hematite, merrillite and late hydrothermal carbonates, silicates and sulfates. Macroscopically, murashkoite is yellowish-grey in colour and has a metallic lustre. In reflected light, the mineral is white with a beige tint and it is non-pleochroic. The anisotropy is distinct, from yellow-grey to greyish-blue. Selected reflectance values [R_{max}–R_{min}, % (λ, nm)] are: 42.7–40.8 (400), 42.0–40.6 (500), 44.5–43.4 (600), 48.0–47.7 (700). It is brittle. VHN_{20} = 468 kg mm^{-2}. The holotype material has the chemical composition (electron microprobe): Fe 63.82; Ni 0.88; P 35.56; total 100.26 wt.%. The empirical formula calculated on the basis of 2 *apfu* is $(Fe_{0.99}Ni_{0.01})_{1.00}P_{1.00}$ corresponding to FeP. Murashkoite is orthorhombic, space group *Pnma*, unit cell parameters refined from the single-crystal data are: *a* 5.099(2), *b* 3.251(2), *c* 5.695(2) Å, *V* 94.41(8) Å^3, *Z* = 4, D_x = 6.108(5) g cm^{-3}. The crystal structure was solved and refined to R_1 = 0.0305 on the basis of 131 unique reflections with $I > 2\sigma(I)$. The strongest lines of the powder X-ray diffraction pattern [(*d*, Å) (*I*, %) (*hkl*)]: 2.831(75)(002,011); 2.548(22)(200); 2.477(46)(102,111); 1.975(47)(112); 1.895(100)(202,211); 1.779(19)(103); 1.632(45)(013,301,020). The mineral is named in honour of Dr. Mikhail Nikolaevich Murashko (born 1952), for his contributions to the mineralogy of the Hatrurim Formation. Murashkoite is a natural counterpart of synthetic FeP, the compound widely used in heterogeneous catalysis and electrocatalysis.

Keywords Iron phosphide · FeP · New mineral · MnP structure type, murashkoite, barringerite · Fe-Ni-P system · Pyrometamorphism · Meteorite · Coal piles · Phosphorylation

Editorial handling: M.A.T.M. Broekmans

Electronic supplementary material The online version of this article (https://doi.org/10.1007/s00710-018-0647-y) contains supplementary material, which is available to authorized users.

✉ Sergey N. Britvin
sergei.britvin@spbu.ru

[1] Institute of Earth Sciences, Saint Petersburg State University, Universitetskaya Nab. 7/9, 199034 St. Petersburg, Russia

[2] Nanomaterials Research Center, Kola Science Center of Russian Academy of Sciences, Fersman Str. 14, 184209 Apatity, Murmansk Region, Russia

[3] Department of Geological and Environmental Sciences, Ben-Gurion University of the Negev, POB 653, 84105 Beer-Sheva, Israel

[4] Geomodel Resource Center, Saint Petersburg State University, Ulyanovskaya Str. 1, 198504 St. Petersburg, Russia

Introduction

Phosphides are a specific class of minerals typical for meteorites but extremely rare on Earth. Natural phosphides belonging to the Fe–Ni–P system are sensitive indicators of the thermal history of metal-rich meteorites, which are considered to be examples of the interior zones of planetary bodies (Scott et al. 2007; Gu et al. 2016). Phosphide minerals attract considerable interest as a likely source of reactive phosphorus required for the processes of prebiotic phosphorylation on the early Earth (Bryant and Kee 2006; Pasek 2017; Pasek et al. 2017; Gull et al. 2015; Horsman and Zechel 2017; Kawamura and Maurel 2017; Kitadai and Maruyama 2018). The most important natural phosphide series is schreibersite–nickelphosphide, Fe_3P–Ni_3P (Clarke and Goldstein 1978; Buchwald 1984;

Published online: 16 November 2018

Britvin et al. 1999). Barringerite, $(Fe,Ni)_2P$ (Buseck 1969), and its high-pressure counterpart allabogdanite $(Fe,Ni)_2P$ (Britvin et al. 2002; Dera et al. 2008) represent another cosmochemically significant phosphide group. Several phosphides sporadically occur as accessory constituents in stony meteorites. These include florenskyite, FeTiP, and andreyivanovite, FeCrP, from the Kaidun polymictic breccia (Ivanov et al. 2000; Zolensky et al. 2008), melliniite, $(Ni,Fe)_4P$, from acapulcoite NWA1054 (Pratesi et al. 2006) and monipite, MoNiP, from the famous Allende CV3 chondrite (Ma et al. 2014). It should be noted that all known meteoritic phosphides are metal-dominant compounds, i.e. those having a *M*/P (metal-to-phosphorus) ratio exceeding unity. Recently, we have described a suite of unusual terrestrial phosphides occurring in the geologically juvenile pyrometamorphic rocks of the Hatrurim Formation (the Mottled Zone), South Levant (the Dead Sea area in Israel and Jordan) (Britvin et al. 2015, 2017, 2018). The remarkable feature of these Earth phosphides is a wide variability of the *M*/P ratios making them substantially distinct from meteoritic minerals. Besides schreibersite, Fe_3P, barringerite, Fe_2P, and zuktamrurite, FeP_2, a new accessory iron phosphide was identified in the rocks of the Mottled Zone having the composition corresponding to FeP. This mineral is named *murashkoite*, in honour of Dr. Mikhail

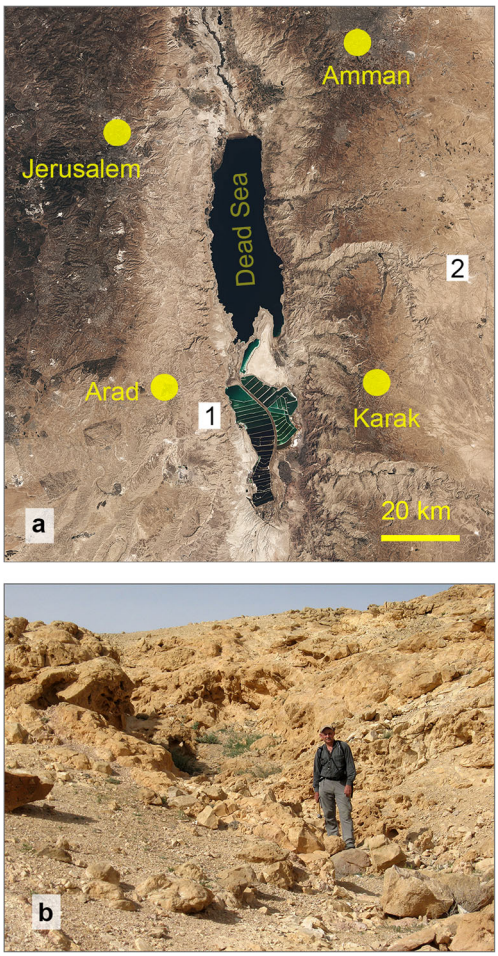

Fig. 1 **a** The Dead Sea area, South Levant, with the numbered locations of murashkoite-bearing outcrops: (1) Halamish wadi, southern part of the Hatrurim Basin, Negev Desert, Israel; (2) Phosphorite quarry at the Daba-Siwaqa locality on the Transjordan Plateau, Jordan. **b** Dr. Mikhail Murashko at the type locality of murashkoite: the Halamish wadi, southern part of the Hatrurim Basin, Negev Desert, Israel. The topographic background for Fig. 1**a** was adapted from the image freely distributed under the Creative Commons Attribution License (CC BY) (https://www.flickr.com/photos/148318224@N03/34460561521)

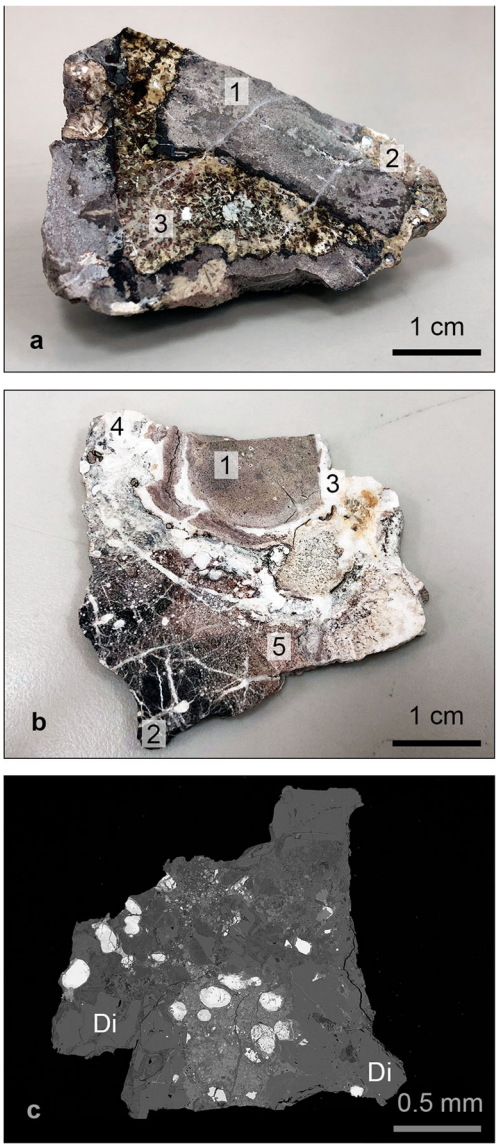

Fig. 2 Typical examples of studied phosphide-bearing rocks. **a** Slice of hydrothermally altered pyrometamorphic marble (field 1) cross-cut by veinlets of altered clinopyroxene-plagioclase paralava (fields 2, 3). Daba-Siwaqa complex, Transjordan Plateau, Jordan. **b** Conglomerate of severely altered marbles cemented by late hydrothermal minerals. Daba-Siwaqa complex, Transjordan Plateau, Jordan. Field numbers (**a**) and (**b**) correspond to the rock compositions presented in Table 2. **c** Ovoidal intergrowths of murashkoite and baringerite (white) in weathered fine-grained diopside (Di) rock. Halamish wadi, southern part of the Hatrurim Basin, Negev Desert, Israel. SEM BSE image

Nikolaevich Murashko (born 1952), a Russian mineralogist, for his contributions to the studies of the Hatrurim Formation. The holotype specimen of murashkoite (IMA 2012–071) is deposited in the collections of the Mineralogical Museum of the Mining Institute (Technical University), St. Petersburg, Russia, catalogue number MGS 2211/1.

Analytical methods

The chemical composition was studied on carbon-coated polished sections by means of an Hitachi S-3400 N scanning electron microscope equipped with an Oxford Instruments AzTec Energy X-Max 20 energy dispersive (EDX) and INCA WAVE 500 wavelength-dispersive (WDX) spectrometers, using the following standards: albite (Na$K\alpha$, Al$K\alpha$, Si$K\alpha$), pyrite (S$K\alpha$), NaCl (Cl$K\alpha$), KCl (K$K\alpha$), wollastonite (Ca$K\alpha$), AsP (P$K\alpha$), Cr metal (Cr$K\alpha$), Fe metal (Fe$K\alpha$), Co metal (Co$K\alpha$) and Ni metal (Ni$K\alpha$). EDX spectra were obtained under the following conditions: 20 kV accelerating voltage, 1 nA beam current, matrix correction by extended Pouchou and Pichoir (XPP) method (Pouchou and Pichoir 1991) which is more accurate than the conventional ZAF correction and implemented in the Oxford Instruments software. Reflectance was measured in air against a Si standard using a MSF-21 spectrophotometer, a monochromator slit of 0.4 mm, 100 μm measured area. X-ray diffraction patterns of rock samples (Table 2) were recorded on a Rigaku Miniflex II diffractometer (Bragg-Brentano geometry), Cu$K\alpha$ radiation and 3 ° min^{-1} scan speed. Subsequent quantitative full-profile Rietveld analyses were carried out using Bruker TOPAS v. 4.2 software (Bruker 2009). X-ray single-crystal and powder diffraction data for murashkoite were collected using a STOE IPDS II diffractometer equipped with a MAR345 flat imaging plate detector, Mo$K\alpha$ radiation (graphite monochromator). The powder pattern was recorded by the Gandolfi method at a crystal-to-detector distance of 200 mm. Calculated intensities and *d*-spacings were obtained by means of CCDC Mercury software (Macrae et al. 2006) using the unit-cell parameters of murashkoite refined from powder data.

Table 1 Chemical composition of pyroxene and plagioclase in the studied phosphide-bearing rocks

Halamish wadi, Hatrurim Basin, Israel			Daba-Siwaqa Complex, Jordan			
	Diopside [a]		Diopside [c]	Hedenbergite [d]	Anorthite [e]	
	Wt.% [b]	Std. dev.	Wt.% [b]	Wt.% [b]	Wt.% [b]	Std. dev.
Na_2O	·		·	·	0.71	0.13
K_2O	·		·	·	0.47	0.11
CaO	25.69	0.64	24.81	22.99	18.39	0.67
MgO	17.74	0.40	17.65	4.15	·	
FeO	0.04	0.00–0.62 [f]	1.42	22.20	·	
Al_2O_3	1.76	0.53	0.97	1.30	32.28	0.55
Fe_2O_3	·		·	·	1.50	0.07 [g]
TiO_2	0.74	0.58	·	·	·	
SiO_2	53.94	1.05	55.31	49.40	46.85	0.90
Total	99.91		100.16	100.04	100.20	
Formula amounts						
	O = 6		O = 6	O = 6	O = 8	
Na	·		·	·	0.04	
K	·		·	·	0.02	
Ca	0.99		0.96	0.98	0.97	
Σ	0.99		0.96	0.98	1.03	
Mg	0.96		0.95	0.25		
Fe^{2+}	·		0.04	0.74		
Ti^{4+}	0.02		·	·		
Σ	0.98		0.99	0.99		
Al	0.07		0.04	0.06	1.79	
Fe^{3+}	·		·	·	0.05	
Si	1.95		1.99	1.97	2.12	
Σ	2.02		2.04	2.03	3.96	

[a] Average of 20 analyses. [b] Middle dot means below detection limit. [c] Max. Mg content found. [d] Max. Fe content. [e] Average of 5 analyses. [f] Range, min–max. [g] Iron is assumed to be ferric based on crystal-chemical considerations

Geological setting and occurrence

Murashkoite was first found in 2011 in the rocks of the Halamish wadi located in the southern part of the Hatrurim Basin, Negev Desert, Israel (31 ° 09′ 47” N, 35 ° 17′ 57″ E, Fig. 1). Three years later, the same mineral was identified in the small phosphorite quarry at the Daba-Siwaqa complex on the Transjordan Plateau, Jordan (31 ° 21′ 52” N, 36 ° 10′ 55″ E, Fig. 1). Both localities have outcrops of metamorphic rocks belonging to the Hatrurim Formation, also known as the “Mottled Zone” (Gross 1977; Burg et al. 1992; Geller et al. 2012). The Hatrurim Formation is the world’s largest sedimentary horizon affected by pyromethamorphic (combustion) alteration. Pyrometamorphism is a process of natural high-temperature calcination and even remelting of the rocks at near atmospheric pressure (Sokol et al. 2005; Grapes 2006). Pyrometamorphic processes are commonly triggered by the local superficial high-temperature events such as volcanic eruptions and subsurface intrusions (Shaw 2009), coal and natural gas combustion (Cosca et al. 1989), and hence are usually confined to relatively local areas. The Hatrurim Formation is a rare exception as its pyrometamorphic rock series is traced over an area exceeding 600 km^2. It is juvenile on the geological timescale having a $^{40}Ar/^{39}Ar$ age between 4.0 and 2.3 Ma (Gur et al. 1995). Outcrops of the Mottled Zone have been reported on both sides of the Dead Sea (Levantine) Transform Fault (Burg et al. 1992). The exact source of heat required for attaining and maintenance of such a high temperature is not completely established; the two competing hypotheses suggest either (1) combustion of bituminous shales (Burg et al. 1992) or (2) firing of methane originating from mud volcanoes (Sokol et al. 2007; Khesin et al. 2010; Novikov et al. 2013). The sediments affected by pyrometamorphism are preferentially Maastrichtian chalks and marls. Metamorphosed phosphorite beds in underlying Campanian layers (Shemesh et al. 1983) may be a possible source of the phosphorus required for the formation of natural phosphides. In extreme cases, extensive melting of the calcined sediments resulted in the formation of the so-called paralavas – pseudo-eruptive rocks often resembling common subvolcanic rock types (Vapnik et al. 2007; Seryotkin et al. 2012). Based on the study of melt inclusions in the paralava minerals, temperatures of formation were estimated as 1150–1200 °C (Sharygin et al. 2006) and even higher at 1280–1350 °C (Sokol et al. 2010). Pyrometamorphic assemblages of the Mottled Zone contain a series of exotic natural refractory oxides: grossite, $CaAl_4O_7$ (Weber and Bischoff 1994); natural ferrites such as barioferrite, $BaFe^{3+}{}_{12}O_{19}$ (Murashko et al. 2010) and harmunite, $CaFe_2O_4$ (Galuskina et al. 2014); perovskite-type

Table 2 Mineral composition of the rock samples depicted on Fig. 2

Mineral	General formula	Mineral content (wt.%)							
		Fields on Fig. 2a			Fields on Fig. 2b				
		1	2	3	1	2	3	4	5
Calcite	$CaCO_3$	30	67	18	79	31	43	36	11
Aragonite	$CaCO_3$	53	·	·	·	·	·	11	61
Plagioclase	$(Ca,Na)Al[(Si,Al)_3O_8]$	·	·	42	·	·	·	·	·
Clinopyroxene	$Ca(Mg,Fe,Al)[(Si,Al)_2O_6]$	·	11	28	·	·	·	·	·
Melilite	$Ca_2(Al,Mg)[(Si,Al)_2O_7]$	·	·	·	·	·	·	11	·
Tridymite	SiO_2	·	·	7	·	·	·	·	·
Cristobalite	SiO_2	·	·	3	·	·	·	·	·
Fluorapatite	$Ca_5(PO_4)_3F$	·	·	2	8	45	·	·	19
Hematite	Fe_2O_3	3	·	·	·	·	·	·	·
Gibbsite	$Al(OH)_3$	·	·	·	·	24	·	·	·
Gypsum	$CaSO_4{\cdot}2H_2O$	·	·	·	2	·	57	8	9
Ettringite	$Ca_6Al_2(SO_4)_3(OH)_{12}{\cdot}26H_2O$	·	·	·	·	·	·	15	·
Phillipsite	$(K_2,Na_2,Ca)[(Si,Al)_8O_{16}]{\cdot}6H_2O$	6	·	·	·	·	·	·	·
Thomsonite	$NaCa_2[Al_5Si_5O_{20}]{\cdot}6H_2O$	8	22	·	·	·	·	·	·
Katoite	$Ca_3Al_2[(SiO_4)_{3-x}(OH)_{4x}]$	·	·	·	11	·	·	·	·
Tobermorite-11 Å	$Ca_5Si_6O_{16}(OH)_2{\cdot}4H_2O$	·	·	·	·	·	·	11	·
Tobermorite-14 Å (Plombierite)	$Ca_5Si_6O_{16}(OH)_2{\cdot}8H_2O$	·	·	·	·	·	·	8	·

Middle dot means not found (below ca. 2 wt.%). The mineral contents were determined via Rietveld refinement of the powder X-ray diffraction data. Accuracy of mineral content determination is ~10 relative %

shulamitite-sharygite series, $Ca_3TiFeAlO_8$ - $Ca_3TiFe_2O_8$ (Sharygin et al. 2013; Juroszek et al. 2018), and vapnikite, Ca_3UO_6 (Galuskin et al. 2014). Complex silico-phosphates, silico-sulfates and silico-vanadates are characteristic accessory phases in the marbles and paralavas of the Mottled Zone (Sokol et al. 2015; Gfeller et al. 2015; Galuskin et al. 2016, 2017 and the references therein). Subsequently, these calcined and remelted rocks of the Hatrurim Formation were subjected to extensive retrograde alteration such as hydrothermal reworking and supergene weathering (Kolodny et al. 2014; Vapnik et al. 2018). In many cases, the marbles and paralavas of the Mottled Zone are completely substituted by a suite of hydrous silicates, carbonates and sulfates.

Mineral assemblages of the host rocks at the two phosphide-bearing localities are substantially different. Rocks outcropping in the quarry at the Daba-Siwaqa complex are represented by centimeter-sized veins of medium-grained paralavas cross-cutting heterogeneous calcined marble conglomerates (Fig. 2a, b). The paralavas are primarily of clinopyroxene-anorthite (gabbro-dolerite)

Table 3 Reflectance values *R* (%) of murashkoite

λ, nm	R_{max}	R_{min}
400	42.7	40.8
420	41.9	40.0
440	41.5	39.8
460	41.6	39.9
480	41.7	40.1
500	42.0	40.6
520	42.2	41.0
540	42.7	41.5
560	43.3	42.1
580	43.9	42.7
600	44.5	43.4
620	45.2	44.3
640	45.9	45.2
660	46.6	46.0
680	47.2	46.9
700	48.0	47.7

Holotype specimen, see the first entry in Table 4

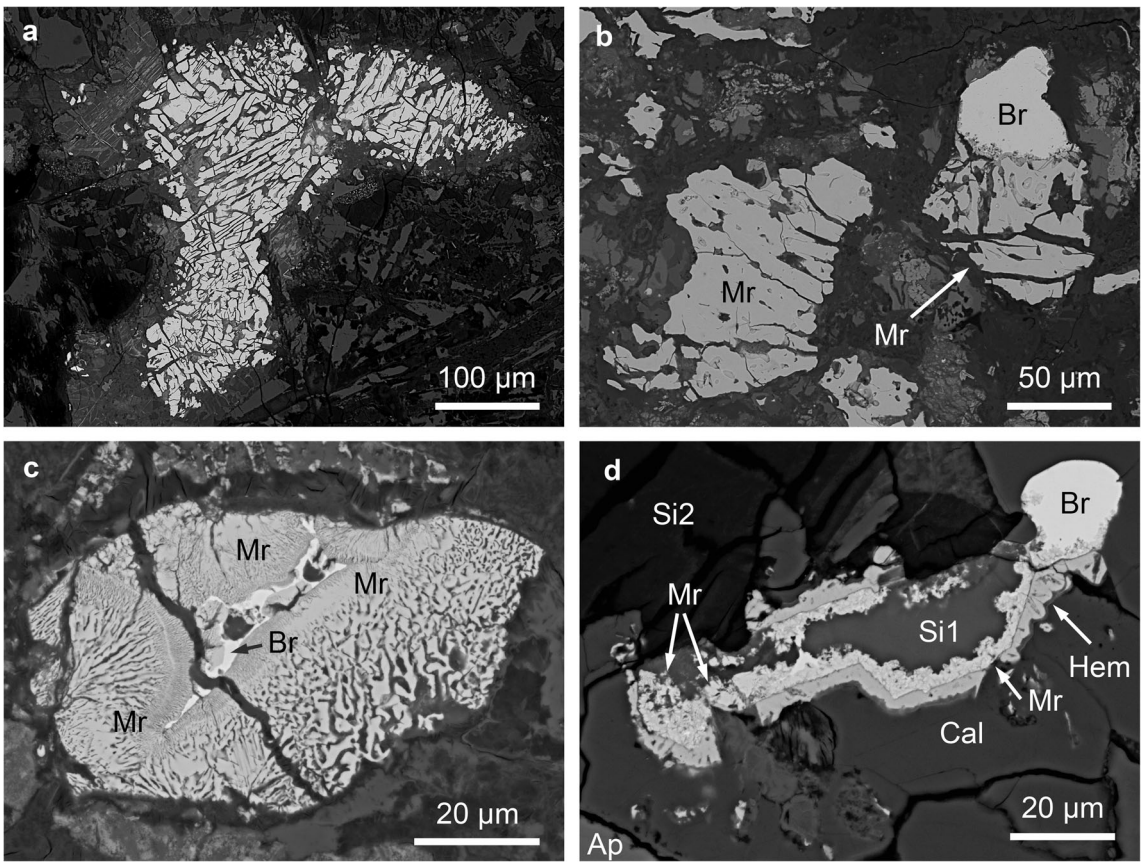

Fig. 3 Murashkoite and its associations. **a** Fractured murashkite grain (light-grey) in a matrix of hydrous silicates and carbonates. **b** Murashkoite grain intergrown with barringerite. **c** Dendritic aggregates of murashkoite in the matrix of hydrous silicates. The central area between dendrites is occupied by barringerite. **d** Tiny crust of murashkoite dendrites grown inwards the pocket filled with the secondary hydrous Fe-Ni silicate. Halamish wadi, southern part of the Hatrurim Basin, Negev Desert, Israel. SEM BSE images. Abbreviations: Mr., murashkoite; Br, barringerite, Di, diopside; Hem, hematite; Ap, fluorapatite; Cal, calcite; Si1, hydrous Fe-Ni silicate; Si2, hydrous Mg-Ca silicate

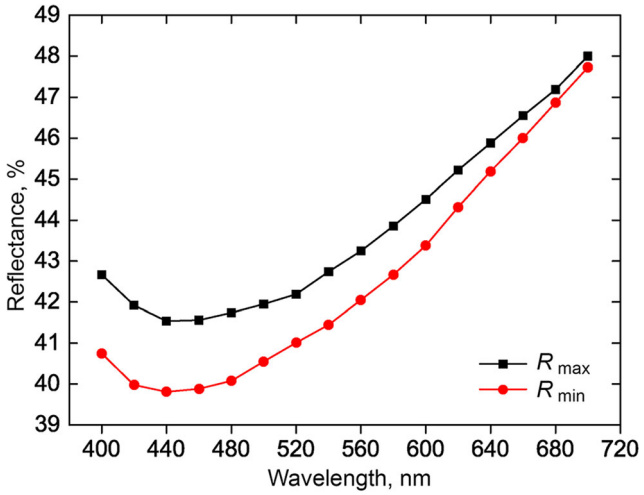

Fig. 4 Reflectance curves of murashkoite

composition (Table 1), bearing a suite of subordinate constituents such as gehlenite, tridymite, cristobalite, accessory magnetite, troilite, pyrrhotite, hematite, merrillite and fluorapatite. Clinopyroxene is rather heterogeneous and varies from diopside to hedenbergite (Table 1) even within one single crystal. Plagioclase has an almost uniform composition approaching the anorthite end-member. This primary association is partially substituted by a low-temperature hydrothermal assemblage consisting of calcite, aragonite, hydrous calcium silicates, zeolites, and gypsum (Table 2). The marble fragments (Fig. 2a, b) are completely replaced by this late association.

The phosphide-bearing rocks at the Halamish wadi (the type locality) (Fig. 2c) consist of fine-grained aggregates of clinopyroxene. In contrast to the pyroxene from the Daba-Siwaqa locality, the latter is rather homogeneous in composition and corresponds to nearly pure diopside, with an insignificant but stable content of titanium (Table 1). Plagioclase was not identified among the seventeen thin sections studied. Accessory minerals include hematite, magnetite, pyrrhotite, merrillite and fluorapatite. Rock samples from the Halamish wadi are severely weathered. The supergene mineral assemblage consists of hydrous X-ray amorphous silicates and hydroxides of Ca, Mg, Fe, Ni, Ca-carbonates and sulfates. These minerals form intimate intergrowths in interstices between diopside grains (Fig. 3).

Appearance and physical properties

Murashkoite usually occurs as isometric grains and aggregates disseminated in the host rock matrix (Fig. 3a). The grain size

Table 4 Representative chemical compositions of murashkoite and associated barringerite

Fe Wt.% [b]	Ni	P	Total	Fe Formula amounts [c]	Ni	P	Fe/(Fe + Ni)	Locality [a]
Murashkoite								
63.82	0.88	35.56	100.26	0.99	0.01	1.00	0.99	1 (holotype)
64.34	·	35.91	100.25	1.00		1.00	1.00	1 (Fig. 3b)
63.44	·	36.24	99.68	0.99		1.01	1.00	1 (Fig. 3c)
63.16	·	36.26	99.42	0.98		1.01	1.00	1 (Fig. 5)
63.32	0.68	36.49	100.49	0.98	0.01	1.01	0.99	2
63.68	1.00	35.49	100.17	0.99	0.01	1.00	0.99	1 (Fig. 3a)
63.43	1.08	34.98	99.49	0.99	0.02	0.99	0.98	1 (Fig. 3d)
60.02	3.63	36.18	99.83	0.93	0.05	1.01	0.95	2
60.05	3.71	36.35	100.11	0.93	0.05	1.02	0.94	1
57.26	6.82	35.43	99.51	0.90	0.10	1.00	0.90	1
55.42	8.32	35.90	99.64	0.87	0.12	1.01	0.88	2
54.00	10.38	35.37	99.75	0.85	0.15	1.00	0.85	1
51.63	13.25	34.84	99.72	0.81	0.20	0.99	0.80	1
Barringerite								
68.63	9.32	22.09	100.04	1.75	0.23	1.02	0.89	1 (Fig. 3b)
70.66	6.96	21.99	99.61	1.81	0.17	1.02	0.91	1 (Fig. 5)
73.57	3.96	22.11	99.64	1.88	0.10	1.02	0.95	1 (Fig. 3d)

[a] Localities: 1, Halamish wadi, southern part of the Hatrurim Basin, Negev Desert, Israel; 2, Daba-Siwaqa Complex, Transjordan Plateau, Jordan. Figure numbers that correspond to the analytical data are given in parentheses. [b] Middle dot means below detection limit. [c] Atoms per formula unit. Recalculated on 2 *apfu* for murashkoite and 3 *apfu* for barringerite

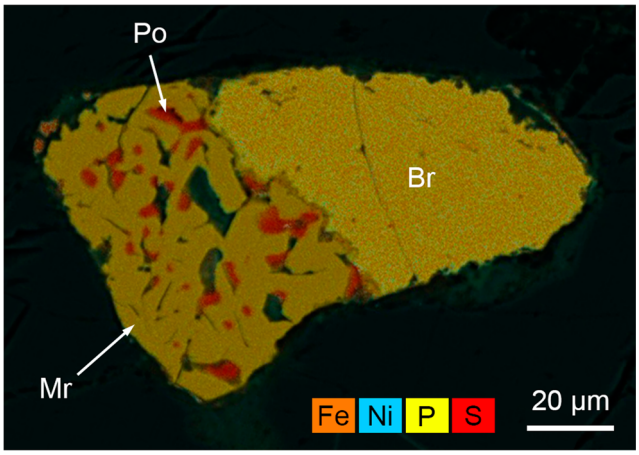

Fig. 5 Murashkoite grain (Mr) containing droplets of pyrrhotite (Po) intergrown with barringerite (Br). Elemental maps in Fe$K\alpha$, Ni$K\alpha$, P$K\alpha$ and S$K\alpha$ superimposed onto grayscale BSE image. Black outer area is hydrous calcium silicates. Halamish wadi, southern part of the Hatrurim Basin, Negev Desert, Israel

may reach 2 mm but typically varies between 10 and 200 μm. The mineral is brittle and the grains are commonly affected by fracturing. Sometimes, the fractures are filled with unidentified secondary hydrous iron phosphates. Murashkoite is commonly associated and intergrown with barringerite, $(Fe,Ni)_2P$ (Fig. 3b). Besides single grains, the mineral frequently forms unusual fine dendritic aggregates composed of submicrometer-sized lamella (Fig. 3b, c). The relationships between murashkoite and barringerite indicate that murashkoite is likely a late mineral relative to barringerite. Macroscopically, murashkoite possesses a yellowish-grey colour with a metallic lustre. In reflected light, the mineral is white with a beige tint and it is non-pleochroic. The bireflectance is weak, ΔR(589 nm) = 0.34%. It is distinctly anisotropic with rotation tints from yellow-grey to greyish-blue. The reflectance values are given in Table 3; the respective reflectance graph is shown on Fig. 4. VHN microhardness (20 g load, average of 7 indentations) is 468 kg mm^{-2} which corresponds to ~5 on Mohs scale.

Table 5 Crystal parameters, data collection and structure refinement details for holotype crystal of murashkoite

Crystal data	
Formula	FeP
Crystal size (mm)	0.05 × 0.06 × 0.12
Crystal system	Orthorhombic
Space group	*Pnma*
a (Å)	5.099(2)
b (Å)	3.251(2)
c (Å)	5.695(2)
V (Å^3)	94.41(8)
Z	4
D_x (g cm^{-3})	6.108(5)
Data collection and refinement	
Radiation	Mo$K\alpha$ (λ = 0.71073 Å)
Temperature (*K*)	273
2Θ range (°)	7.2–56.00
Total reflections collected	1403
Unique reflections	134
Unique observed $I \geq 2\sigma(I)$	131
$R_{int.}$	0.1397
R_σ	0.0442
h, k, l range	−6 → 6, −4 → 4, −7 → 7
R_1 [$F \geq 4\sigma(F)$]	0.0305
R_1 (all data)	0.0317
wR_2	0.0654
S = *GoF*	1.214

Table 6 Powder X-ray diffraction data for murashkoite

I_{obs}	d_{obs} (Å)	I_{calc}	d_{calc} (Å)	*h k l*
5	3.805	5	3.800	1 0 1
		13	2.850	0 0 2
75	2.831	50	2.824	0 1 1
22	2.548	19	2.549	2 0 0
		13	2.487	1 0 2
46	2.477	29	2.470	1 1 1
		1	2.327	2 0 1
		5	2.006	2 1 0
47	1.975	32	1.975	1 1 2
		35	1.900	2 0 2
100	1.895	100	1.892	2 1 1
19	1.779	21	1.780	1 0 3
		2	1.640	2 1 2
		28	1.640	0 1 3
45	1.632	11	1.628	3 0 1
		25	1.626	0 2 0
4	1.524	2	1.523	2 0 3
4	1.454	2	1.456	3 1 1
4	1.413	4	1.412	0 2 2
		1	1.379	2 1 3
7	1.370	2	1.372	1 0 4
		4	1.371	2 2 0
6	1.361	2	1.361	1 2 2
6	1.276	5	1.275	4 0 0
		4	1.267	3 0 3
12	1.264	10	1.264	1 1 4
		1	1.244	2 0 4
11	1.235	15	1.235	2 2 2
6	1.199	8	1.200	1 2 3
		3	1.163	4 0 2
9	1.163	9	1.162	4 1 1

Table 7 Fractional atomic coordinates and displacement parameters (Å^2) in the crystal structure of murashkoite

Site [a]	*x/a*	*y/b*	*z/c*	U_{iso}	U_{11}	U_{22}	U_{33}	U_{13}
Fe (4*c*)	0.0015(2)	1/4	0.2007(2)	0.0124(3)	0.0076(4)	0.0147(5)	0.0149(5)	0.0000(3)
P (4*c*)	0.1926(3)	1/4	0.5775(3)	0.0131(4)	0.0115(6)	0.0121(8)	0.0158(7)	0.0000(7)

[a] Site multiplicities and Wyckoff symbols are given in parentheses. $U_{23} = 0$ and $U_{12} = 0$ by default

Chemical composition

The relative abundance of accessory murashkoite allowed reliable statistical data on its chemical composition to be determined. Representative electron microprobe (EDX mode) analyses of the mineral are given in Table 4. From more than 100 analytical points, the data for Table 4 were stepwise selected based on Fe/(Fe + Ni) atomic ratio with the step size of 0.05. Chemical composition of the holotype specimen (Table 4) corresponds to almost pure FeP. Our results indicate the existence of a discontinuous FeP–NiP solid solution containing up to 0.20 Ni atoms per formula unit (~13 wt.% Ni). The grains of murashkoite are chemically homogeneous and do not show zoning or variations in the Fe/Ni ratio (Fig. 5). Murashkoite is always depleted in Ni relative to associated barringerite, as can be seen from the analyses in Table 4. The remarkable chemical feature of murashkoite is that the mineral does not contain detectable cobalt. The Co content in the studied grains is always below the detection limit of the energy-dispersive spectrometer (0.1 wt.%) (Table 4). Selected analyses for Co by means of a wavelength-dispersive spectrometer showed that the Co content in murashkoite is below 0.05 wt.%.

Crystal structure and related minerals

Crystal parameters, general data collection and structure refinement details for the holotype crystal of murashkoite are summarized in Table 5. Data integration and processing routines were performed by means of a STOE X-Area v. 1.42 program package (Stoe and Cie 2006). The crystal structure was solved by direct methods and refined to $R_1 = 0.0305$ using a *SHELX*-2014 program suite (Scheldrick 2015) and Olex2 v.1.2.8 graphical user interface (Dolomanov et al. 2009). Further details of data processing and refinement are given in the Supplementary Information (Crystallographic Information File (CIF)). Powder X-ray diffraction data for murashkoite were obtained from the same single crystal used for single-crystal X-ray data collection (Table 6). The indexing and least-squares refinement of the powder pattern resulted in the following unit-cell parameters: *a* 5.098(5), *b* 3.251(1), *c* 5.699(3) Å, $V = 94.5(2)$ Å^3, $Z = 4$, which are in good agreement with single-crystal data. Murashkoite crystallizes in the MnP (B31) structure type (Schonberg 1954), which is an orthorhombically distorted homeotype of the hexagonal aristotype structure of nickeline, NiAs (B8 type) (Makovicky 2006). In general, among phosphides of

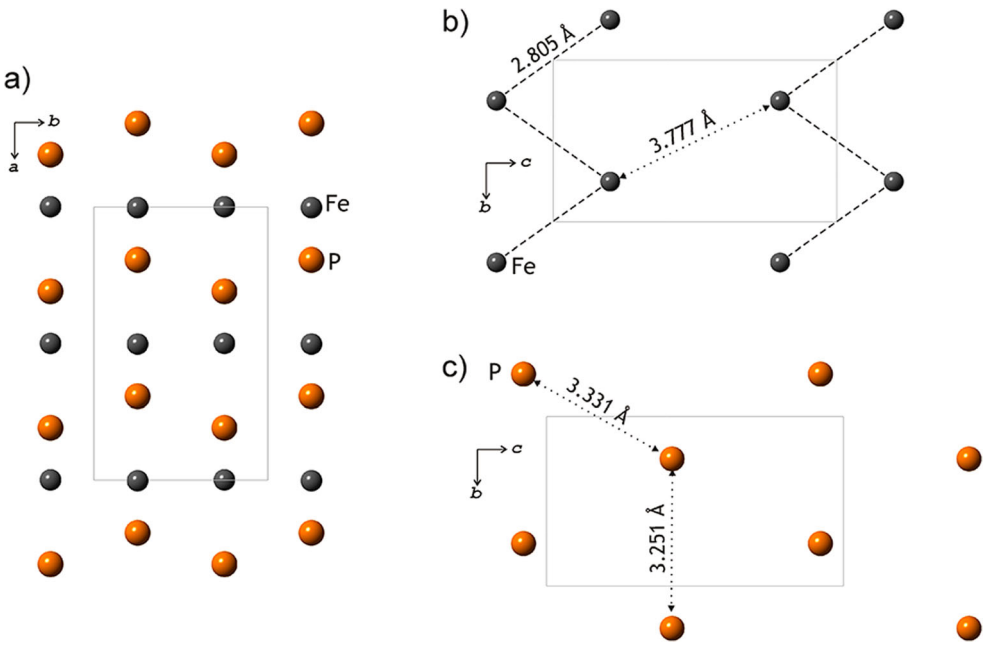

Fig. 6 Arrangement and bonding of P and Fe in the crystal structure of murashkoite

transitional metals M with the [Ar]$3d^n4s^2$ electronic configurations ($n = 2$–8; M = Ti, V, Cr, Mn, Fe, Co, Ni), the TiP (n = 2) and VP ($n = 3$) adopt ideal NiAs (B8) structure type, whereas CrP, MnP, FeP, and CoP ($n = 4$–7) crystallize in the distorted B31 structure type (space group *Pnma*). In contrast, the ambient-pressure polymorph of NiP with the valence-shell configuration $3d^84s^2$ (or $3d^94s^1$) crystallizes in the *Pbca* space group and is also a distorted derivative of the $B8_1$ structure type (Larsson 1965; Dera et al. 2011). Tremel et al. (1986) analyzed the electronic structure of transitional metal phosphides MP with M = Ti-Ni and demonstrated that structure deformation associated with the transition from the NiAs to MnP structure type is driven by a second-order Jahn-Teller-like distortion, stabilized by the formation of M-M bonds, whereas the MnP → NiP transition is associated with the formation of bonds between pairs of metal and phosphorus atoms (Tables 7 and 8).

By analogy with the crystal structure of NiAs, the crystal structure of murashkoite is based upon layers of Fe and P atoms alternating along the *a* axis (which, in this respect, is analogous to the *c* axis in NiAs) (Fig. 6a). The layer of Fe atoms is a distorted planar 3^6 net consisting of chains of Fe-Fe atoms with Fe-Fe distances of 2.805 Å extended along the *b* axis (Fig. 6b). The layer of P atoms is a non-planar 3^6 net with no P-P contacts shorter than 3 Å (Fig. 6c). In general, the coordination of Fe can be described as a distorted [FeP_6] octahedron complemented by four additional Fe-Fe bonds of 2.611 and 2.805 Å (Fig. 7a). The P site is in distorted trigonal prismatic coordination by six Fe atoms complemented by two P-P contacts of 2.698 Å (Fig. 7b). The pronounced Fe–Fe interactions in murashkoite (Table 8) are noticeably shorter than the corresponding Fe-Fe bonds in the crystal structure of troilite, FeS (2.93–2.99 Å), which crystallizes in the undistorted NiAs structure type (Makovicky 2006). Tremel et al. (1986) pointed out that the metal-metal and P-P bonds in MnP and NiP are critical for the stabilization of these structure types.

Table 8 Selected interatomic distances in the crystal structure of murashkoite

Site 1	Site 2	Distance (Å)
Fe	P	1 × 2.2341(19)
Fe	P	2 × 2.2842(14)
Fe	P	1 × 2.357(2)
Fe	P	2 × 2.3594(14)
Fe	Fe	2 × 2.6107(10)
Fe	Fe	2 × 2.8046(17)

The upper limit for the isomorphous substitution of Fe for Ni in the studied murashkoite samples corresponds to ~20 mol% of NiP (Table 4). The lack of further enrichment in nickel may be explained by geochemical arguments, i.e. the deficit of Ni in the whole mineral system. On the other hand, the maximum Ni content in murashkoite may be limited by crystal chemical and electronic features. There are four NiP polymorphs known and none of them crystallizes in the B31 structure type (Dera et al. 2011, 2013), which explains the existence of a miscibility gap in the FeP–NiP solid solutions. Murashkoite is the phosphide analogue of westerveldite, FeAs (Oen et al. 1972), and belongs to the modderite mineral group, which now includes five distinct mineral species (Table 9). Among them, murashkoite is the only phosphide found in Nature.

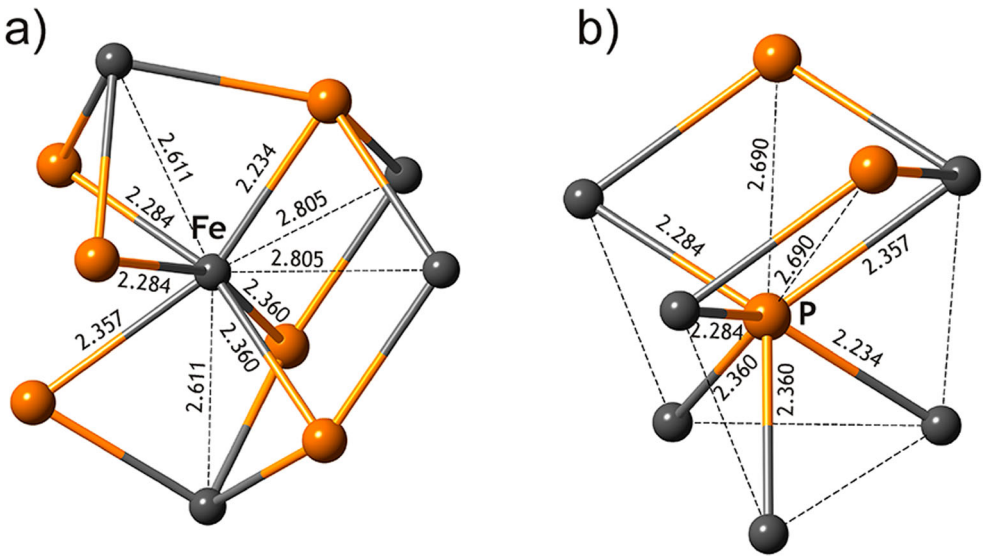

Fig. 7 The building units of the murashkoite structure: **a** distorted [FeP_6] octahedron and **b** distorted trigonal prism [PFe_6]

Table 9 Comparative cell metrics of murashkoite and related arsenide minerals

Mineral	Formula	*a* (Å)	*b* (Å)	*c* (Å)	Reference
Murashkoite	FeP	5.099	3.251	5.695	This work
Westerveldite	FeAs	5.33	3.45	5.97	Oen et al. 1972
Modderite	CoAs	5.2857	3.4883	5.8675	Lyman and Prewitt 1984 [a]
Ruthenarsenite	RuAs	5.628	3.239	6.184	Harris 1974
Cherepanovite	RhAs	5.70	3.59	6.00	Rudashevsky et al. 1985

All minerals crystallize in the orthorhombic system, space group *Pnma*, $Z = 4$

[a] Data for synthetic analogue

Discussion

The conditions required for the formation of murashkoite in nature include high temperature, a reducing environment and sources of phosphorus and iron. It has been shown that a mixture of synthetic FeP (murashkoite) and Fe_2P (barringerite) can be obtained in one step via direct reduction of whitlockite-type phosphate $Ca_9Fe^{3+}(PO_4)_7$ at 550 °C in an H_2 atmosphere (Lazoryak et al. 2003). Minerals of the merrillite–ferromerrillite series $Ca_9Na(Mg,Fe)(PO_4)_7$ (Britvin et al. 2016) which are related to the whitlockite group, were identified among the phosphates associated with murashkoite. These minerals might be the precursors for the formation of phosphides in the studied mineral associations. At the same time, any natural association of fluorapatite with iron oxides could also serve as a source of P and Fe. The reducing agent could be methane (Burns et al. 2007), dihydrogen gas or burning carbonaceous (bituminous) matter (Prins and Bussell 2012). The high nickel contents in the paralavas of the Hatrurim Formation and the surrounding rocks were reported and their origin was thoroughly discussed (Fleurance et al. 2013). Therefore, the conditions appropriate for the direct geosynthesis of phosphides coincide well with the geochemical situation expected during combustion metamorphism of the Mottled Zone. However, the oxidative environment of the contemporary Earth's crust fulfils these requirements very rarely. The *P–T* conditions favourable for the formation of phosphides are typical for coal combustion processes: the technogenic analogue of murashkoite has been described from the burning coal piles in the Chelyabinsk region, Urals, Russia (Nishanbaev et al. 2002). Otherwise, the reported occurrences of terrestrial phosphides are confined to a few very local points (Pedersen 1981; Borodaev et al. 1982; Yang et al. 2005; Pasek and Block 2009; Plyashkevich et al. 2016). However, it is likely that highly reducing conditions of the early Earth (Horita and Berndt 1999; Fiebig et al. 2007) could promote the formation of terrestrial phosphides, which, in due course, could serve as a source of low-valent phosphorus required for prebiotic phosphorylation processes (Britvin et al. 2015). Recent studies aimed at simulation of oxidative phosphorylation are focused on the phosphides related to the shreibersite–nickelphosphide (Fe_3P–Ni_3P) series (Bryant et al. 2013; Pirim et al. 2014; La Cruz et al. 2016; Pasek et al. 2007; Pasek 2017). It is known, however, that synthetic FeP, a counterpart of murashkoite, is a rather reactive phosphide substantially overcoming Fe_3P in the processes of heterogeneous catalysis, photo- and electrocatalysis (Jiang et al. 2014; Callejas et al. 2014). Considering the Mottled Zone localities as models of the Archean Earth's phosphide geosynthesis, one could expect that phosphorus-rich phosphides like murashkoite could also play a role in the source of prebiotic phosphorus as well.

Acknowledgements This research was supported by the Russian Science Foundation (grant 18-17-00079). The authors thank the Resource Center of X-ray diffraction studies and "Geomodel" Resource Centre of Saint-Petersburg State University for providing instrumental and computational resources. The authors gratefully acknowledge Dr. Chris Stanley and Dr. Evgeny Galuskin for the helpful comments and discussion of the manuscript.

References

Borodaev YS, Bogdanov YA, Vyal'sov LN (1982) New nickel-free variety of schreibersite Fe_3P. Zapiski VMO 111:682–687 (Russian)

Britvin SN, Kolomensky VD, Boldyreva MM, Bogdanova AN, Kretser YL, Boldyreva ON, Rudashevsky NS (1999) Nickelphosphide (Ni, Fe)$_3$P – the nickel analog of schreibersite. Zapiski VMO 64–72(Russian):128

Britvin SN, Rudashevsky NS, Krivovichev SV, Burns PC, Polekhovsky YS (2002) Allabogdanite, $(Fe,Ni)_2P$, a new mineral from the Onello meteorite: the occurrence and crystal structure. Am Mineral 87: 1245–1249

Britvin SN, Murasko MN, Vapnik Y, Polekhovsky YS, Krivovichev SV (2015) Earth's phosphides in Levant and insights into the source of Archaean prebiotc phosphorus. Sci Rep 5:8355

Britvin SN, Krivovichev SV, Armbruster T (2016) Ferromerrillite, $Ca_9NaFe^{2+}(PO_4)_7$, a new mineral from the Martian meteorites, and some insights into merrillite-tuite transformation in shergottites. Eur J Mineral 28:125–136

Britvin SN, Murashko MN, Vapnik E, Polekhovsky YS, Krivovichev SV (2017) Barringerite Fe_2P from pyrometamorphic rocks of the Hatrurim Formation, Israel. Geol Ore Deposit 59: 619–625

Britvin SN, Murashko MN, Vapnik E, Polekhovsky YS, Krivovichev SV, Vereshchagin OS, Vlasenko NS, Shilovskikh VV, Zaitsev AN (2018) Zuktamrurite, FeP_2, a new mineral, the phosphide analogue of löllingite, $FeAs_2$. Phys Chem Minerals. https://doi.org/10.1007/s00269-018-1008-4

Bruker AXS (2009) Topas 4.2. General profile and structure analysis software for powder diffraction data. Karlsruhe, Germany

Bryant DE, Kee TP (2006) Direct evidence for the availability of reactive, water soluble phosphorus on the early Earth. H-Phosphinic acid from the Nantan meteorite. Chem Commun 2006:2344–2346

Bryant DE, Greenfield D, Walshaw RD, Johnson BRG, Herschy B, Smith C, Pasek MA, Telford R, Scowen I, Munshi T, Edwards HGM, Cousins CR, Crawford IA, Kee TP (2013) Hydrothermal modification of the Sikhote-Alin iron meteorite under low pH geothermal environments. A plausibly prebiotic route to activated phosphorus on the early Earth. Geochim Cosmochim Acta 109:90–112

Buchwald VF (1984) Handbook of Iron meteorites. University of California Press

Burg A, Starinsky A, Bartov Y, Kolodny Y (1992) Geology of the Hatrurim formation ("Mottled Zone") in the Hatrurim basin. Isr J Earth Sci 40:107–124

Burns S, Hargreaves JSJ, Hunter SM (2007) On the use of methane as a reductant in the synthesis of transition metal phosphides. Catal Commun 8:931–935

Buseck PR (1969) Phosphide from meteorites: barringerite, a new iron-nickel mineral. Science 165:169–171

Callejas JF, McEnaney JM, Read CG, Crompton JC, Biacchi AJ, Popczun EJ, Gordon TR, Lewis NS, Schaak RE (2014) Electrocatalytic and photocatalytic hydrogen production from acidic and neutral-pH aqueous solutions using Iron phosphide nanoparticles. ACS Nano 8:11101–11107

Clarke RS Jr, Goldstein JI (1978) Schreibersite growth and its influence on the metallography of coarse-structured iron meteorites. Smithson Contrib Earth Sci (21):1–80

Cosca MA, Essene EJ, Geissman JW, Simmons WB, Coates DA (1989) Pyrometamorphic rocks associated with naturally burned coal beds, Powder River Basin, Wyoming. Am Mineral 74:85–100

Dera P, Lavina B, Borkowski LA, Prakapenka VB, Sutton SR, Rivers ML, Downs RT, Boctor NZ, Prewitt CT (2008) High-pressure polymorphism of Fe_2P and its implications for meteorites and Earth's core. Geophys Res Lett 35:L10301

Dera P, Lazarz JD, Lavina B (2011) Pressure-induced development of bonding in NiAs type compounds and polymorphism of NiP. J Solid State Chem 184:1997–2003

Dera P, Nisar J, Ahuja R, Tkachev S, Prakapenka VB (2013) New type of possible hige-pressure polymorphism in NiAs minerals in planetary cores. Phys Chem Miner 40:183–193

Dolomanov OV, Bourhis LJ, Gildea RJ, Howard JA, Puschmann H (2009) OLEX2: a complete structure solution, refinement and analysis program. J Appl Crystallogr 42:339–341

Fiebig J, Woodland AB, Spangenberg J, Oschmann W (2007) Natural evidence for rapid abiogenic hydrothermal generation of CH4. Geochim Cosmochim Acta 71:3028–3039

Fleurance S, Cuney M, Malartre F, Reyx J (2013) Origin of the extreme polymetallic enrichment (Cd, Cr, Mo, Ni, U, V, Zn) of the Late Cretaceous–Early Tertiary Belqa Group, central Jordan. Palaeogeogr Palaeoclimatol Palaeoecol 369:201–219

Galuskin EV, Galuskina IO, Kusz J, Armbruster T, Marzec KM, Dzierzanowski P, Murashko M (2014) Vapnikite Ca_3UO_6 a new double-perovskite mineral from pyrometamorphic larnite rocks of the Jabel Harmun, Palestinian Autonomy, Israel. Mineral Mag 78:571–581

Galuskin EV, Galuskina IO, Gfeller F, Kruger B, Kusz J, Vapnik Y, Dulski M, Dzierzanowski P (2016) Silicocarnotite, $Ca_5[(SiO_4)(PO_4)](PO_4)$, a new ,,old" mineral from the Negev Desert, Israel, and the ternesitesilicocarnotite solid solution: indicators of high-temperature alteration of pyrometamorphic rocks of the Hatrurim Complex, Southern Levant. Eur J Mineral 28:105–123

Galuskin EV, Gfeller F, Galuskina IO, Armbruster T, Krzatala A, Vapnik Y, Kusz J, Dulski M, Gardocki M, Gurbanov AG, Dzierzanowski P (2017) New minerals with a modular structure derived from hatrurite from the pyrometamorphic rocks. Part III. Gazeevite, $BaCa_6(SiO_4)_2(SO_4)_2O$, from Israel and the Palestine Autonomy, South Levant, and from South Ossetia, Greater Caucasus. Mineral Mag 81:499–514

Galuskina IO, Vapnik Y, Lazic B, Armbruster T, Murashko M, Galuskin EV (2014) Harmunite $CaFe_2O_4$: a new mineral from the Jabel Harmun, West Bank, Palestinian autonomy, Israel. Am Mineral 99:965–975

Geller YI, Burg A, Halicz L, Kolodny Y (2012) System closure during the combustion metamorphic "Mottled Zone" event, Israel. Chem Geol 334:25–36

Gfeller F, Widmer R, Krüger B, Galuskin EV, Galuskina IO, Armbruster T (2015) The crystal structure of flamite and its relation to Ca_2SiO_4 polymorphs and nagelschmidtite. Eur J Mineral 27:755–769

Grapes R (2006) Pyrometamorphism. Springer-Verlag, Berlin Heidelberg

Gross S (1977) The mineralogy of the Hatrurim Formation, Israel. Bull Geol Surv Israel 70:1–80

Gu T, Fei Y, Wu X, Qin S (2016) Phase stabilities and spin transitions of $Fe_3(S_{1-x}P_x)$ at high pressure and its implications in meteorites. Am Mineral 101:205–210

Gull M, Mojica MA, Fernandez FM, Gaul DA, Orlando TM, Liotta CL, Pasek MA (2015) Nucleoside phosphorylation be the mineral schreibersite. Sci Rep-UK 5:17198

Gur D, Steinitz G, Kolodny Y, Starinsky A, McWilliams M (1995) $^{40}Ar/^{39}Ar$ dating of combustion metamorphism ("Mottled Zone", Israel). Chem Geol 122:171–184

Harris DC (1974) Ruthenarsenite and iridarsenite, two new minerals from the territory of Papua and New Guinea and associated irarsite, laurite and cubic iron-bearing platinum. Can Mineral 12:280–284

Horita J, Berndt ME (1999) Abiogenic methane formation and isotopic fractionation under hydrothermal conditions. Science 285:1055–1057

Horsman GP, Zechel DL (2017) Phosphonate biochemistry. Chem Rev 117:5704–5783

Ivanov AV, Zolensky ME, Saito A, Ohsumi K, Yang SV, Kononkova NN, Mikouchi T (2000) Florenskyite, FeTiP, a new phosphide from the Kaidun meteorite. Am Mineral 85:1082–1086

Jiang P, Liu Q, Liang Y, Tian J, Asiri AM, Sun X (2014) A cost-effective 3D hydrogen evolution cathode with high catalytic activity: FeP nanowire Array as the active phase. Angew Chem Int Ed 53:12855–12859

Juroszek R, Krüger H, Galuskina I, Krüger B, Jeżak L, Ternes B, Wojdyla J, Krzykawski T, Pautov L, Galuskin E (2018) Sharyginite, $Ca_3TiFe_2O_8$, a new mineral from the Bellerberg volcano, Germany. Minerals 8:308

Kawamura K, Maurel M-C (2017) Walking over 4 Gya: chemical evolution from photochemistry to mineral and organic chemistries leading to an RNA world. Orig Life Evol Biosph 47:281–296

Khesin B, Vapnik Y, Itkis S (2010) Case history. Geophysical evidence of deep hydrocarbon flow in Mottled Zone areas, Dead Sea Transform zone. Geophysics 75:B91–B101

Kitadai N, Maruyama S (2018) Origins of building blocks of life: a review. Geosci Front 9:1117–1153

Kolodny Y, Burg A, Geller YI, Halicz L, Zakon Y (2014) Veins in the combusted metamorphic rocks, Israel; weathering or a retrograde event? Chem Geol 385:140–155

La Cruz NL, Qasim D, Abbott-Lyon H, Pirim C, McKee AD, Orlando T, Gull M, Lindsay D, Pasek MA (2016) The evolution of the surface of the mineral schreibersite in prebiotic chemistry. Phys Chem Chem Phys 18:20160–20167

Larsson E (1965) An X-ray investigation of the Ni-P system and the crystal structures of NiP and NiP_2. Ark Kemi 23:335–356

Lazoryak BI, Belik AA, Kotov RN, Leonidov IA, Mitberg EB, Karelina VV, Kellerman DG, Stefanovich SY, Avetisov AK (2003) Reduction and Re-? Oxidation behavior of calcium iron phosphate, $Ca_9Fe(PO_4)_7$. Chem Mater 15:625–631

Lyman PS, Prewitt CT (1984) Room- and high-pressure crystal chemistry of CoAs and FeAs. Acta Cryst B 40:14–20

Ma C, Beckett JR, Rossman GR (2014) Monipite, MoNiP, a new phosphide mineral in a Ca-Al-rich inclusion from the Allende meteorite. Am Mineral 99:198–205

Macrae CF, Edgington PR, McCabe P, Pidcock E, Shields GP, Taylor R, Towler M, van de Streek J (2006) Mercury: visualization and analysis of crystal structures. J Appl Crystallogr 39:453–457

Makovicky E (2006) Crystal structures of sulfides and other chalcogenides. Rev Mineral Geochem 61:7–125

Murashko MN, Chukanov NV, Mukhanova AA, Vapnik E, Britvin SN, Krivovichev SV, Polekhovskii YS, Ivakin YD (2010) Barioferrite BaFe3+12O19 – a new magnetoplumbite-group mineral from Hatrurim formation, Israel. Zapiski VMO 139:22–31 (Russian)

Nishanbaev TP, Rochev AV, Kotlyarov VA (2002) Iron phosphides from the burned coal dumps of Chelyabinsk coal basin. Uralsky Geol J 25(1):105–114 (Russian)

Novikov I, Vapnik Y, Safonova I (2013) Mud volcano origin of the Mottled Zone, south Levant. Geosci Front 4:597–619

Oen IS, Burke EAJ, Kieft C, Westerhof AB (1972) Westerveldite (Fe,Ni,Co) As, a new mineral from La Gallega, Spain. Am Mineral 57:354–363

Pasek MA (2017) Schreibersite on the early Earth: scenarios for prebiotic phosphorylation. Geosci Front 8:329–335

Pasek M, Block K (2009) Lightning-induced reduction of phosphorus oxidation state. Nat Geosci 2:553–556

Pasek MA, Dworkin JP, Lauretta DS (2007) A radical pathway for organic phosphorylation during schreibersite corrosion with implications for the origin of life. Geochim Cosmochim Acta 71:1721–1736

Pasek MA, Gull M, Herschy B (2017) Phosphorylation on the early earth. Chem Geol 475:149–170

Pedersen AK (1981) Armalcolite-bearing Fe-Ti oxide assemblages in graphite equilibrated salic volcanic rocks with native iron from Disko, Central West Greenland. Contrib Mineral Petrol 77:307–324

Pirim C, Pasek MA, Sokolov DA, Sidorov AN, Gann RD, Orlando TM (2014) Investigation of schreibersite and intrinsic oxidation products from Sikhote-Alin, Seymchan, and Odessa meteorites and Fe_3P and Fe_2NiP synthetic surrogates. Geochim Cosmochim Acta 140:259–274

Plyashkevich AA, Minyuk PS, Subbotnikova TV, Alshevsky AV (2016) Newly formed minerals of the Fe-P-S system in Kolyma fulgurite. Dokl Earth Sci 467(2):380–383

Pouchou JL, Pichoir F (1991) Quantitative analysis of homogeneous or stratified microvolumes applying the model "PAP". In: Heinrich KFJ, Newbury DE, Eds., Electron Probe Quantitation, New York

Pratesi G, Bindi L, Moggi-Cecci V (2006) Icosahedral coordination of phosphorus in the crystal structure of melliniite, a new phosphide mineral from the northwest Africa 1054 acapulcoite. Am Mineral 91:451–454

Prins R, Bussell ME (2012) Metal phosphides: preparation, characterization and catalytic reactivity. Catal Lett 142:1413–1436

Rudashevsky NS, Motshalov AG, Trubkin NV, Shumskaya NM, Shkursky VI, Evstigneeva TL (1985) Cherepanovite RhAs – a new mineral. Zapiski VMO 114:464–469 (Russian)

Scheldrick GM (2015) Crystal structure refinement with SHELXL. Acta Cryst C71:3–8

Schonberg N (1954) An X-ray investigation of transition metal phosphides. Acta Chem Scand 3:226–239

Scott HP, Huggins S, Frank MR, Maglio SJ, Martin CD, MengY SJ, Williams Q (2007) Equation of state and high-pressure stability of Fe_3P-schreibersite: implications for phosphorus storage in planetary cores. Geophys Res Lett 34:L06302

Seryotkin YV, Sokol EV, Kokh SN (2012) Natural pseudowollastonite: crystal structure, associated minerals, geological context. Lithos 134–135:75–90

Sharygin VV, Vapnik Y, Sokol EV, Kamenetsky VS, Shagam R (2006) Melt inclusions in minerals of schorlomite-rich veins of the Hatrurim Basin, Israel: composition and homogenization temperatures. ACROFII program with abstracts, Nanjing University PH. China:189–192

Sharygin VV, Lazic B, Armbruster TM, Murashko MN, Wirth R, Galuskina IO, Galuskin EV, Vapnik Y, Britvin SN, Logvinova AM (2013) Shulamitite $Ca_3TiFe^{3+}AlO_8$ – a new perovskite-related mineral from Hatrurim Basin, Israel. Eur J Mineral 25:97–111

Shaw CSJ (2009) Caught in the act – the first few hours of xenolith assimilation preserved in lavas of the Rockeskyllerkopf volcano, West Eifel, Germany. Lithos 112:511–523

Shemesh A, Kolodny Y, Luz B (1983) Oxygen isotope variations in phosphate of biogenic apatites, II. Phosphorite rocks. Earth Planet Sci Lett 64:405–416

Sokol EV, Maksimova NV, Nigmatulina EN, Sharygin VV, Kalugin VM (2005) Combustion metamorphism. Publishing House of the SB RAS–Novosibirsk, 284 p (Russian)

Sokol EV, Novikov IS, Vapnik Y, Sharygin VV (2007) Gas fire from mud volcanoes as a trigger for the appearance of high-temperature pyrometamorphic rocks of the Hatrurim Formation (Dead Sea area). Dokl Earth Sci 413A:474–480

Sokol E, Novikov I, Zateeva S, Vapnik Y, Shagam R, Kozmenko O (2010) Combustion metamorphic rocks as indicators of fossil mud volcanism: new implications for the origin of the Mottled Zone, Dead Sea rift area. Basin Res 22:414–438

Sokol EV, Seryotkin YV, Kokh SN, Vapnik Y, Nigmatulina EN, Goryainov SV, Belogub EV, Sharygin VV (2015) Flamite, $(Ca,Na,K)_2(Si,P)O_4$, a new mineral from ultrahightemperature combustion metamorphic rocks, Hatrurim Basin, Negev Desert, Israel. Mineral Mag 79:583–596

Stoe & Cie (2006). X-AREA and X-RED32. Stoe & Cie, Darmstadt, Germany

Tremel W, Hoffmann R, Silvestre J (1986) Transitions between NiAs and MnP type phases: an electronically driven distortion of triangular (36) nets. J Am Chem Soc 108:5174–5187

Vapnik Y, Sharygin V, Sokol E, Shagam R (2007) Paralavas in a combustion metamorphic complex, Hatrurim Basin, Israel. GSA Rev Eng Geol XVIII:133–153

Vapnik Y, Palchika V, Galuskina I, Banasik K, Krzykawski T (2018) Mineralogy, chemistry and rock mechanic parameters of katoite-bearing rock from the Hatrurim Basin, Israel. J. Afr. Earth Sci 147: 322–330

Weber D, Bischoff A (1994) Grossite ($CaAl_4O_7$) - a rare phase in terrestrial rocks and meteorites. Eur J Mineral 6:591–594

Yang JS, Bai WJ, Rong H, Zhang ZM, Xu ZQ, Fang QS, Yang BG, Li TF, Ren YF, Chen SY, Hu J-Z, Su JF, Mao HK (2005) Discovery of Fe_2P alloy in garnet peridotite from the Chinese continental scientific drilling project (CCSD) main hole. Acta Petrol Sin 21:271–276

Zolensky M, Gounelle M, Mikouchi T, Ohsumi K, Le L, Hagiya K, Tachikawa O (2008) Andreyivanovite: a second new phosphide from the Kaidun meteorite. Am Mineral 93:1295–1299